Hindawi
International Journal of Polymer Science
Volume 2021, Article ID 7339812, 22 pages
https://doi.org/10.1155/2021/7339812

Research Article

The Curing Kinetics of Multiscale $[Ni(EDTA)]^{-2}$ Intercalated Zn-Al Layered Double Hydroxides: Glass Fiber–Epoxy Composite Prepreg

Reza Darvishi,[1] **Mahdi Darvishi**,[2] **and Ali Moshkriz**[3]

[1]*Polymer Engineering Department, Faculty of Petroleum and Gas (Gachsaran), Yasouj University, Gachsaran 75813-56001, Iran*
[2]*School of Railway Engineering, Iran University of Science and Technology, Tehran, Iran*
[3]*Department of Chemical Engineering, Faculty of Engineering, Arak University, Arak 38156-8-8349, Iran*

Correspondence should be addressed to Reza Darvishi; r.darvishi@yu.ac.ir

Received 16 July 2021; Revised 29 October 2021; Accepted 2 November 2021; Published 10 December 2021

Academic Editor: Domenico Acierno

In the present research, the effect of Zn_2Al layered double hydroxides (LDH) and nickel (II)-EDTA complex intercalated LDH (LDH-$[Ni(EDTA)]^{-2}$) on the cure kinetics of glass fiber/epoxy prepreg (GEP) was explored using nonisothermal differential scanning calorimetry (DSC). The results showed that LDH caused a shift in the cure temperature toward lower temperatures while accelerating the curing of epoxy prepregs. The use of LDH-$[Ni(EDTA)]^{-2}$ more profoundly influenced the acceleration of the curing process. The curing kinetics of prepregs was assessed through the differential isoconversional Friedman (FR) technique and the integration method of Flynn–Wall–Ozawa (FWO) and Kissinger–Akahira–Sunose (KAS). A decrease was detected in the E_α value of glass fiber/LDH-$[Ni(EDTA)]^{-2}$/epoxy (GELP) and glass fiber/LDH-$[Ni(EDTA)]^{-2}$/epoxy (GELNiP) prepregs at small cure degrees relative to GEP, suggesting the catalytic effect of LDH or LDH-$[Ni(EDTA)]^{-2}$ on the initial epoxy/amine reaction. Furthermore, LDH-$[Ni(EDTA)]^{-2}$ performed better due to the catalyst role of nickel (II). Moreover, the activation energy exhibited lower reliance on the degree of conversion in the cases of GELP and GELNiP rather than pure epoxy prepregs. An autocatalytic model was used to evaluate the curing behavior of the system. Based on the results, the curing reaction of the epoxy prepreg can be described by the autocatalytic Šesták-Berggren model even after the incorporation of LDH or LDH-$[Ni(EDTA)]^{-2}$. The kinetic parameters of the autocatalytic model (such as E_α, A, m, n) and the equations explaining the curing behavior of prepregs were introduced as well whose predictions were in line with the experimental findings.

1. Introduction

Glass fiber/epoxy prepregs have been extensively utilized in the structures of automobiles as well as aerospace and space industries owing to their excellent strength-to-weight ratios and proper thermal and electrical features [1–3]. The ongoing works in the field of composites show that further modification of the systems with nanomaterials could improve their other characteristics such as the interlaminar strength of laminated composites through prepregs. Recently, the nanosized fillers have been incorporated in the prepregs [4–9]. The nanoengineered hybrid epoxy composite laminates include three components: regular reinforcing fibers/fabrics, nanofillers, and epoxy resins. These structures can be fabricated by two general methods; incorporation of nanofillers in the epoxy resin and using the resultant modified epoxy resin to prepare the composite laminate or the introduction of nanofillers on the reinforcing fabric and/or into the interlaminar zone prior to preparing the composite laminate [10, 11]. The layered double hydroxides (LDHs) belong to a class of nanofillers in which positively charged metal hydroxide layers are rested on the brucite structures with intercalated hydrated anions. LDHs are also regarded as hydrotalcite-like compounds or anionic clays with the general formula of $[M^{II}_{1-x}M^{III}_{x}(OH)_2](A^{n-}_{x/n}.mH_2O)$, in which M^{II} and M^{III} refer to divalent and trivalent metal

cations, respectively, occupying the octahedral positions within the hydroxide layers. A^{n-} also denotes an interlayer hydrated anion compensating for the layer charge [12]. LDHs can serve as molecular sieves, adsorbents, and catalysts in diverse chemical reactions [10]. Based on their degree of intercalation, exfoliation, and dispersion, the nanosized inorganic LDHs can make a remarkable improvement in thermal stability [12], mechanical features [13], flame retardancy behavior [14], and UV absorption [15] of neat polymeric matrix/composites, even at relatively small amounts. The organic intercalation of LDH seems to be an efficient approach to improve their compatibility with epoxy and augment their dispersion within the epoxy matrix [11]. As documented, the characteristics of the epoxy-based composites strongly depend on the curing reactions and the extent of 3D network formation during the curing process [2, 16–19]. Curing dramatically alters the thermal, physical, and mechanical features of the system depending on the kinetics of the curing process [1, 20, 21]. The curing process includes a series of complex reactions whose complete investigation requires considering the reactants, curing agent, crosslinkers, catalysts, and products. Regarding the potential impact of the original and organically intercalated on curing kinetics, study of the curing process at their presence could provide valuable information on the chemical reactions and hence deeper understanding of structure-related characteristics of such composites [20]. In the course of thermosetting matrix composite preparation, the reinforcing fibers and nanoparticles restrain the molecular movements of the resin matrix. Despite no changes in the curing mechanism of the resin, some heat released from the resin will be absorbed by the fibers and nonoparticles, leading to a drastic difference in the kinetic parameters of the prepreg and neat resin. Precise curing kinetic parameters are required for prediction of the behavior of the multiscale nanoparticles/fiberglass/epoxy composite preprege during a particular curing cycle. Generally, the extent of improvement in the mechanical and thermal properties of the thermoset nanocomposites has a strong dependence on the curing state [21]. The theoretical models can precisely describe the curing of composite prepreg using the experimental curing findings from differential scanning calorimetry (DSC) [22]. As a thermoanalytical method, DSC correlates the heat flow variations with the resin reaction rates in the course of curing. Dynamic DSC measures the heat flow and total heat flow rates in terms of temperature to offer information with higher reliability compared to the isothermal modes [6, 22, 23]. The curing degree (α) is directly related to the ratio of the crosslinking released heat by (ΔH_t) to the total amount of heat produced throughout the reaction (i.e., $\alpha = (\Delta H_t/\Delta H_{\text{total}})$) [24].The curing heat can be determined through integration over the entire heat flow curve. N^{th} and autocatalytic models with the respective curing conversion-dependence functions of $f(\alpha) = (1-\alpha)^n$ and $f(\alpha) = \alpha^m(1-\alpha)^n$, as well as their combination, are among the various kinetic models of DSC cure analysis capable of predicting the characteristics of the cured system at a particular cure cycle [25, 26]. The m and n represent the symmetry and shape of the curve of the reaction rate, respectively. The kinetic analyses can be categorized to the model-fitting and model-free schemes. The former requires a proper model for determining the kinetic parameters (e.g., activation energy, conversion equation, and frequency factor) through mathematical optimization methods with the use of experimental from no-isothermal DSC assessments. In the model-free (isoconversional) methods, the curing reaction rate at a definite conversion (α) only relies on temperature. These methods can be classified into two groups; the differential methods such as Friedman (FR) and the integral techniques including Flynn–Wall–Ozawa (FWO) and Kissinger–Akahira–Sunose (KAS) [7, 18, 19]. The errors due to the improper models or parameters should be avoided to reach more accurate activation energies with no interference with the dynamic model functions. Similar kinetic parameters are attained by fitting under isothermal or nonisothermal evaluations; hence, the isothermal curing behavior can be described using nonisothermal data. The variation of the conversion temperature can be determined by [17]

$$\frac{d\alpha}{dT} = \frac{Ae^{-E_a/RT}f(\alpha)}{\varphi}. \tag{1}$$

Using the isoconversional differential methods, the FR model can be expressed as [24]

$$\ln\left(\frac{d\alpha}{dT}\varphi\right) = \ln(A) + \ln(f(\alpha)) - \frac{E_a}{RT}, \tag{2}$$

in which φ shows the heating rate (dT/dt), $(d\alpha/\text{dT}) \times \varphi$ represents the curing rate ($d\alpha/dt$), A denotes a preexponential factor, and R and T are the gas constant (8.314 J/mol) and the absolute temperature (K). E_α stands for the activation energy which alters by curing degree. $f(\alpha)$ does not depend on the heating cycle. The activation energy E_α for various curing degrees (α) could be determined through linear regression of $\ln((d\alpha/dT)\varphi)$ and T^{-1} at different heating rates for diverse curing degrees [18].

The FWO method uses the isoconversional integral method. The kinetic equation can be attained by the approximate solution of the temperature integral function in equation (3) [7, 27, 28]:

$$\ln(\varphi) = \ln\left(\frac{0.0048AE_a}{Rf(\alpha)}\right) - \frac{1.052E_a}{RT}. \tag{3}$$

The activation energy for different curing degrees can be determined through the linear fitting of the $\ln(\varphi)$ and the T^{-1} at different heating rates and curing degrees. With the help of isoconversional integral method, KAS can determine the kinetic equation by approximately solving the temperature integral function in equation (4) [7]:

$$\ln\left(\frac{\varphi}{T^{1.92}}\right) = \ln\left(\frac{AE_a}{Rf(\alpha)}\right) - \frac{1.0008E_a}{RT}. \tag{4}$$

The activation energy E_a for various curing degrees can be attained through linear regression of $\ln(\varphi/T^{1.92})$ and T^{-1} at different heating rates.

Many studies have addressed the curing kinetics of glass fiber/epoxy [1, 9] and LDH/epoxy systems [11]. However, the three-component multiscale LDH/fiberglass/epoxy composite prepreg systems have been rarely investigated. Karami et al. [29] examined the curing potential of the HA-functionalized LDH/epoxy nanocomposites and reported that the kinetics determined by the model-free methods are autocatalytic. Hayaty et al. [30, 31] and Gerami et al. [24] explored the curing reaction of glass/fiber prepreg and determined the autocatalytic model for the kinetics of both systems. Previous studies indicate that curing kinetic models of the glass/epoxy prepreg are mainly autocatalytic with constant activation energies. Nonetheless, the activation energy of LDH/epoxy systems showed drastic variations in the course of the curing reaction. To our knowledge, there are no studies investigating the curing kinetics of a multiscale LDH/glass/epoxy prepreg. In this context, the present study is aimed at evaluating the influence of Zn_2/Al-LDH and $[Ni(EDTA)]^{2-}$ complex intercalated Zn2/Al-LDH (nano)particles on the cure kinetics of glass fiber epoxy in prepreg composites. To this end, three-phase multiscale prepreg was fabricated based on diglycidyl ether of bisphenol A (DGEBA), glass fiber, and LDH (nano)particles. The dynamic DSC was then employed to study the curing activities of the specimens. The variations in the activation energy of samples throughout the curing reactions were examined by isoconversional methods of Friedman (FR), Kissinger-Akahira-Sunose (KAS), and Flynn-Wall-Ozawa (FWO). Further kinetic evaluations were achieved by calculating activation energy ($E\alpha$), frequency factor, and the orders of autocatalytic reactions throughout the curing process.

2. Experimental

2.1. Materials. Epoxy resin (EEW: 174 g/eq) and m-phenylenediamine (MPD, 99%) were supplied by Sigma-Aldrich. Aceton (Merck Co.) was utilized as the solvent. The commercial glass fiber fabric (SAERTEX; and weight of 301 g/m^2) included two layers of E-glass fibers laid at ±45° upon each other.

2.2. Differential Scanning Calorimetry (DSC). The curing features of the prepregs were assessed by a DSC (Netsch, 200-F3 Maia, Germany) at the heating rates of 5, 10, 15, and 20 K/min under N_2 atmosphere. An empty cell was used as a reference in the temperature range of 25 to 320°C. The heat flow was normalized to the weight of the samples (4–5 mg). Nitrogen was purged at the rate of 40 mL min^{-1} to minimize the oxygen accessibility.

2.3. Synthesis of LDH

2.3.1. Synthesis of Zn_2/Al-NO_3-LDH. The initial LDHs, [Zn_2/Al-NO_3] which was employed in the anion-exchange reaction, was prepared through the following stages: 12.1 g $Al(NO_3)_3{\cdot}9H_2O$ and 19.1 g $Zn(NO3)_2$. $6H_2O$ was dissolved in 100 mL deionized and decarbonated water to reach the total Zn: Al ratio of 2. The obtained solution was then dropwise added to 50 mL aqueous solution of 12.5% wt NaOH and 18.2% wt $NaNO_3$ under stirring. The reaction mixture underwent stirring at 60°C until full precipitation. The pH was kept at 8-9 using NaOH solution. The obtained gel-like slurry underwent aging at 60°C for 24 h which was then collected by vacuum filtration after cooling down followed by washing with hot DD water and drying at 65°C for minimum 12 hours, obtained LDH.

2.3.2. Synthesis of Ni^{2+} Intercalation in [Zn2/Al–EDTA]. The ethylenediaminetetraacetate (EDTA) intercalated LDHs were synthesized through the coprecipitation approach as mentioned elsewhere [32]. In a typical procedure, a solution containing 1.8 g $Al(NO_3)_3{\cdot}9H_2O$ and 3.5 g $Zn(NO_3)_2{\cdot}6H_2O$ was made in 150 mL of deionized (DI) water. Afterward, the pH of EDTA aqueous solution (0.1 M) was set to ~7 using NaOH solution which was dropwise added to 150 mL of a metal solution under stirring to maintain the pH at the optimum level (8 to 9). The obtained gel-like slurry underwent overnight aging at 70°C, followed by filtration and several times washing with DI water and air drying at 65°C for 12 h. In the next step, 2 g coprecipitated [Zn_2/Al–EDTA] was dispersed in 50 mL of the Ni^{2+}nitrate salt solution. The solution concentration was set at 0.05 M. The suspensions were occasionally shaken at room temperature for 24 h. The obtained solids were filtered, washed with DI water, and air-dried at room temperature. The resulting powder product was named as LDH-[Ni (EDTA)]$^{-2}$.

2.4. LDH and LDH-[Ni (EDTA)]$^{-2}$ Characterization. The powder X-ray diffraction (XRD) analysis was carried out using Shimadzu X-ray Diffractometer XRD-7000, with monochromatic Cu Kα radiation ($\lambda = 1.5418$ Å) at 40 kV and 30 mA and the dwell time of 1° min^{-1}. Fourier transform infrared (FTIR) spectroscopy (Perkin Elmer; Spectrume GX) was also applied using the KBr pellet technique. The data were recorded at resolution of 2 cm over a wavenumber region of 400–4000 cm^{-1}.

2.5. Preparation of Prepregs. LDH and LDH-[Ni (EDTA)]$^{2-}$ were initially dispersed in acetone followed by 30 minutes of sonication. Subsequently, the (nano)particle suspension was mixed with the epoxy solution in acetone. m-Phenylenediamine (MPD) underwent 20 minutes of premelting at 115°C followed by 30 minutes of high-shear mixing with epoxy/(nano)particle suspension (100 : 15) to reach proper homogeneity. The final content of (nano)particles in the epoxy/MPD matrix was 0.2%wt. Afterward, square patches of commercial glass fiber fabric (31 × 31 cm^2) were successively put on a flat glass panel and uniformly brushed with the (nano)particle-containing epoxy/MPD/acetone blend. The prepregs were then placed in an oven at 50°C for 30 min to enhance their wettability and eliminate any residual solvent. The specimens were labeled as GEP (glass fiber/epoxy prepreg), GELP (glass fiber/epoxy/LDH prepreg), and GELNiP (glass fiber/epoxy/LDH-[Ni(EDTA)]$^{-2}$ prepreg). The prepregs were kept at -10°C until further evaluations.

3. Result and Discussion

3.1. LDH Characterization. Figure 1 depicts the FTIR results of LDH and LDH-[Ni(EDTA)]$^{2-}$.

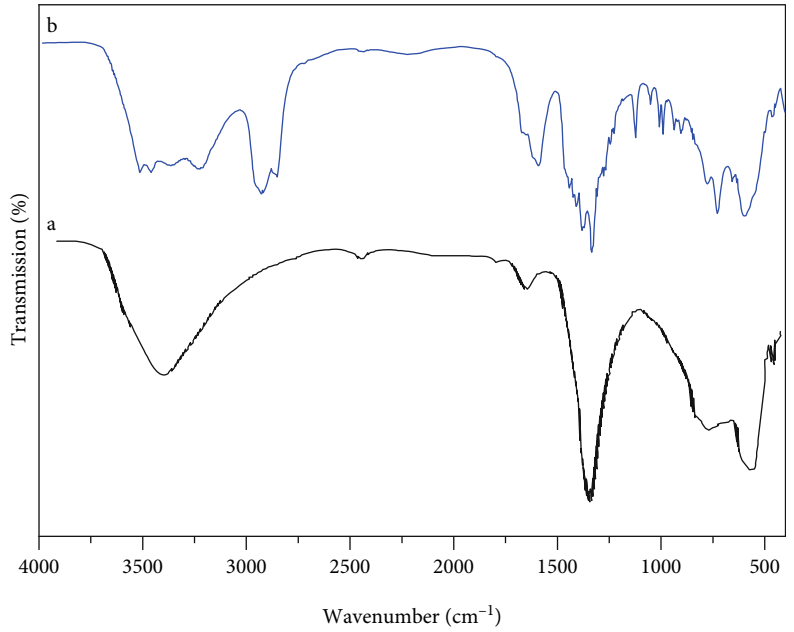

Figure 1: The FT-IR spectra of (a) LDH and (b) LDH-[Ni(EDTA)]$^{2-}$.

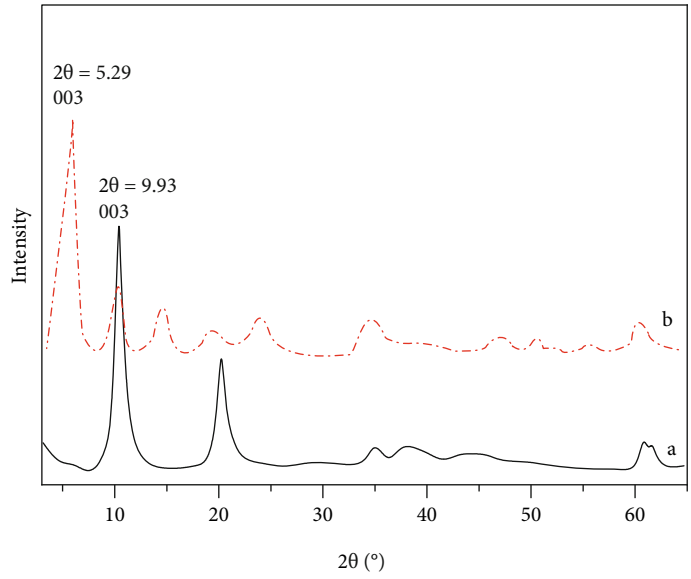

Figure 2: The powder XRD patterns of (a) LDH and (b) LDH-[Ni(EDTA)]$^{-2}$.

In the case of LDH, the peak at 3400 cm^{-1} can be assigned to the O-H vibrations in the hydroxyl groups and H_2O. A weak absorption at 1630 cm^{-1}in the FTIR spectra can be ascribed to the H_2O bending vibration of the interlayer water. The peaks at 460, 550, and 790 cm^{-1} are related to the Al-O condensed groups, Zn/Al-OH translation, and the Al-OH deformation, respectively [33]. A strong signal at about 1380 cm^{-1} also signifies the antisymmetric stretching mode (υ3) of the nitrate anion in the LDH intercalated with NO_3.Considering LDH-[Ni(EDTA)]$^{-2}$, the new signals at 1120 cm^{-1} can be ascribed to the bending vibrations as a consequence of EDTA and Ni^{2+}coordination. The peaks at 1750 and 1629 cm^{-1} also reflect the stretching vibrations of carbonyl and the Ni-capped carboxylic groups in EDTA, respectively [34]. The new peaks at 1400 cm^{-1} can be assigned to the stretching vibration of the amine group.

The XRD patterns of Zn_2Al-LDH-NO_3 (LDH) and the [Ni(EDTA)]$^{-2}$ intercalated LDH (LDH-[Ni(EDTA)]$^{-2}$) are presented in Figure 2.

The sharp peaks indicate the highly ordered and regular stacking of the LDH layers. In the case of LDH, the peaks can be well assigned to hexagonal the structure planes of

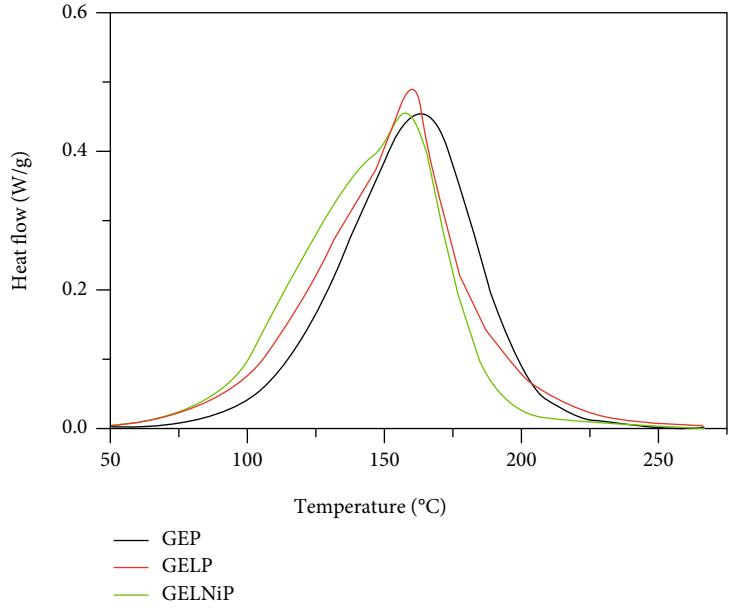

(a)

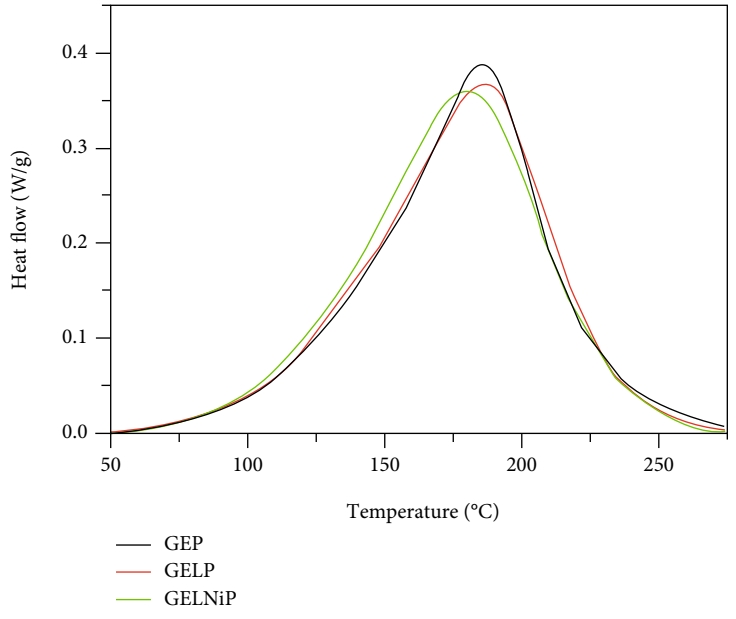

(b)

Figure 3: Continued.

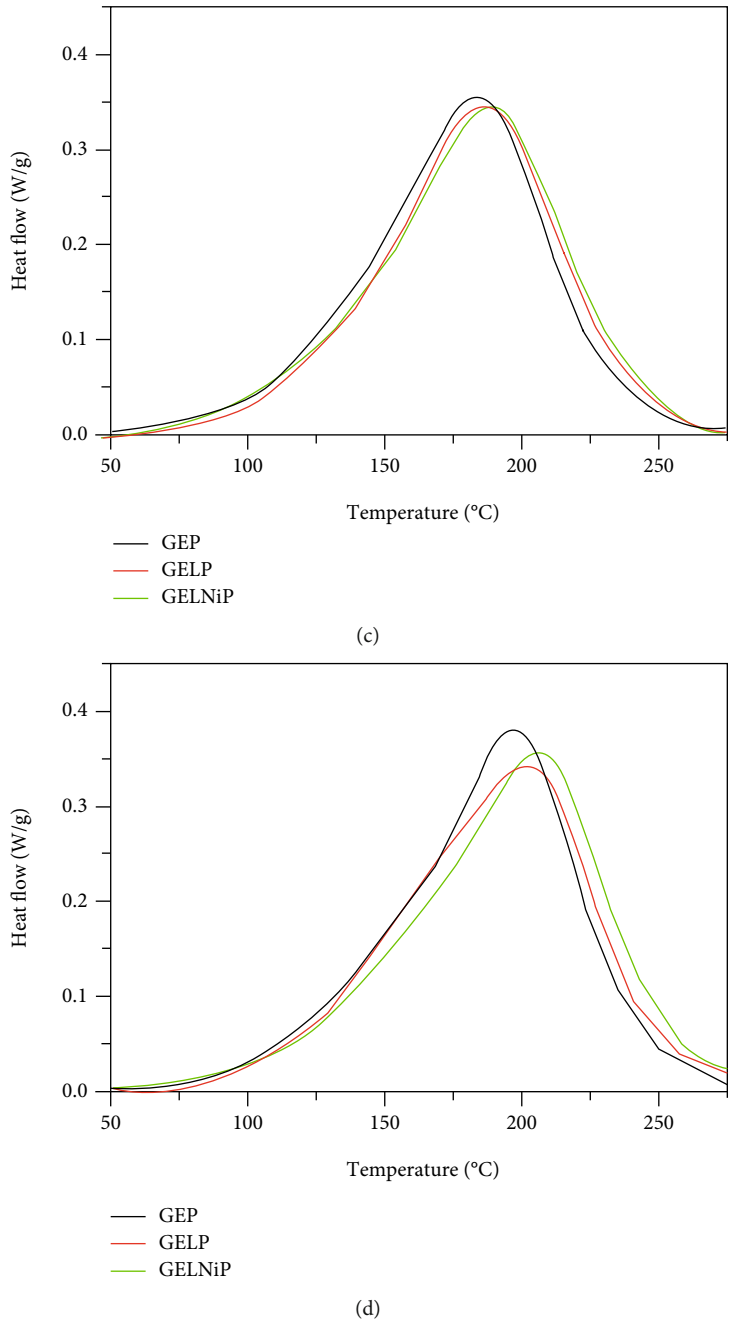

Figure 3: Cure state of GEP and GELP and GELNiP nanocomposites at heating rates of (a) 5, (b)10, (c) 15, and (d) 20°C/min.

(003), (006), and (009) [33], with the basal spacing of 0.890 nm for (003). An increment can be detected in the basal distance of LDH-$[Ni(EDTA)]^{-2}$ (Figure 2(b)) which can be attributed to the complex $[Ni(EDTA)]^{-2}$ intercalation. A basal spacing shift can be observed from 0.89 nm for LDH to 2.55 nm for LDH-$[Ni(EDTA)]^{-2}$complex implying the $[Ni(EDTA)]^{-2}$ intercalation in the galleries.

3.2. Curing Characteristics for the GEP, GELP, and GELNiP. Figure 3 shows the DSC curves of the GEP, GELP, and GELNiP at various heating rates. The conversion $\alpha(T)$ can be observed in terms of temperature for GEP, GELP, and GELNiP for various heating rates.

The obtained diagrams can be exploited to calculate the kinetic parameters of the curing process. Due to its aromatic primary amines, curing of epoxy is a highly complex polyaddition procedure which may involve secondary amine addition. At advanced stages or higher temperatures, side reactions (e.g., etherification or homopolymerization) are also probable. The differences in the DSC curves of the epoxy prepregs indicate the profound impact of LDH or LDH-$[Ni\ (EDTA)]^{-2}$ on the curing procedure. The LDH altered the onset (T_o), peak (T_p), and end (T_e) temperatures

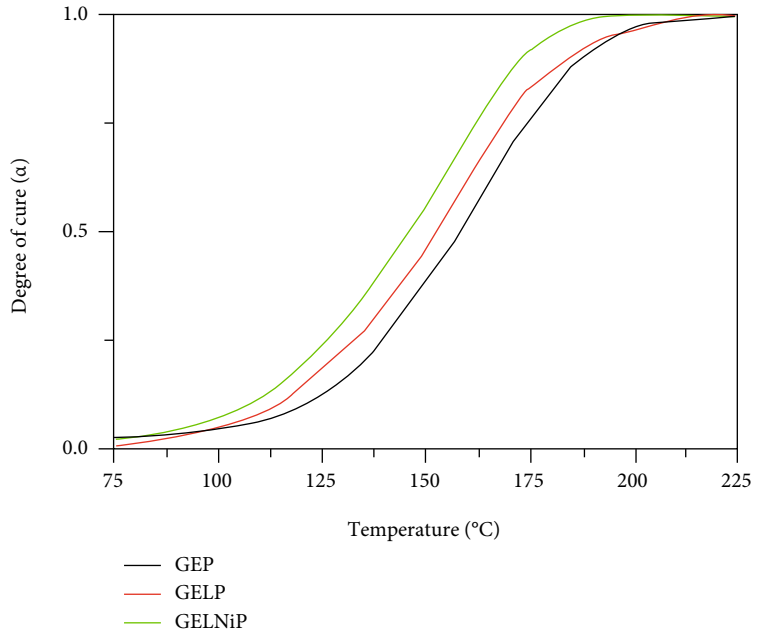

(a)

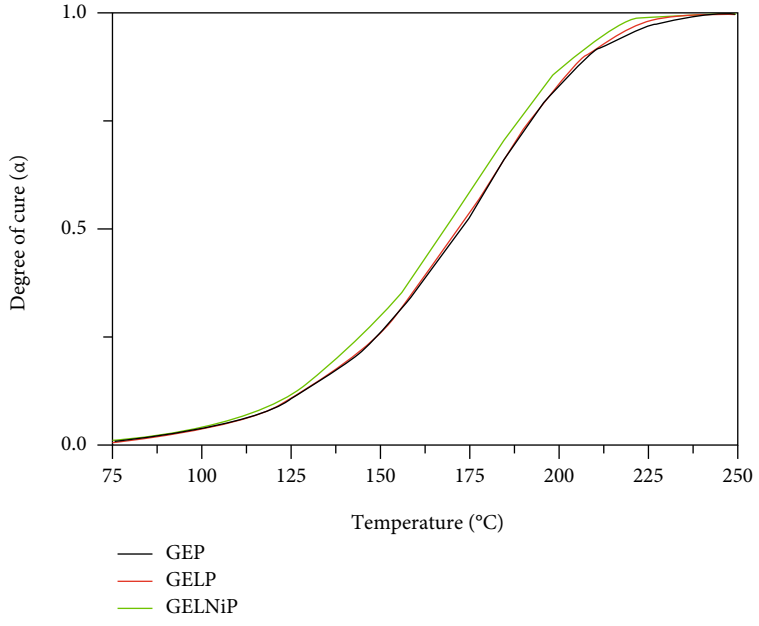

(b)

Figure 4: Continued.

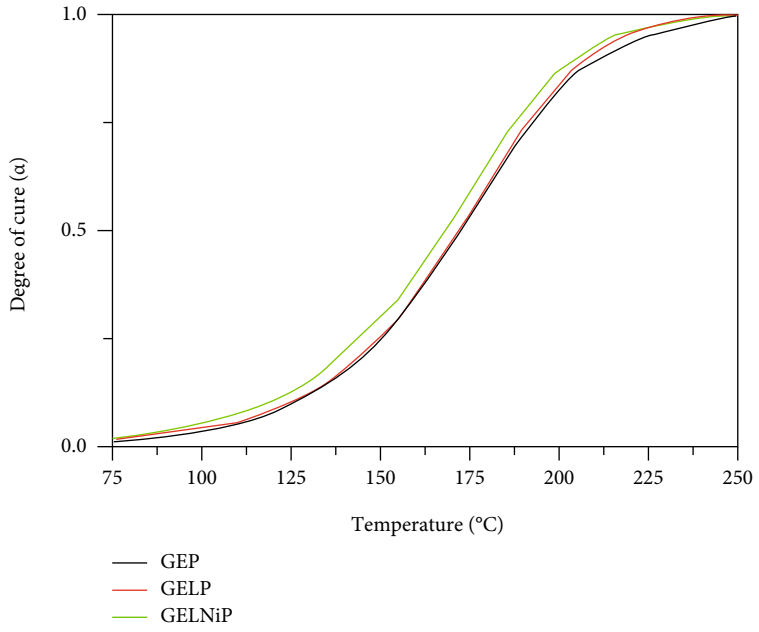

(c)

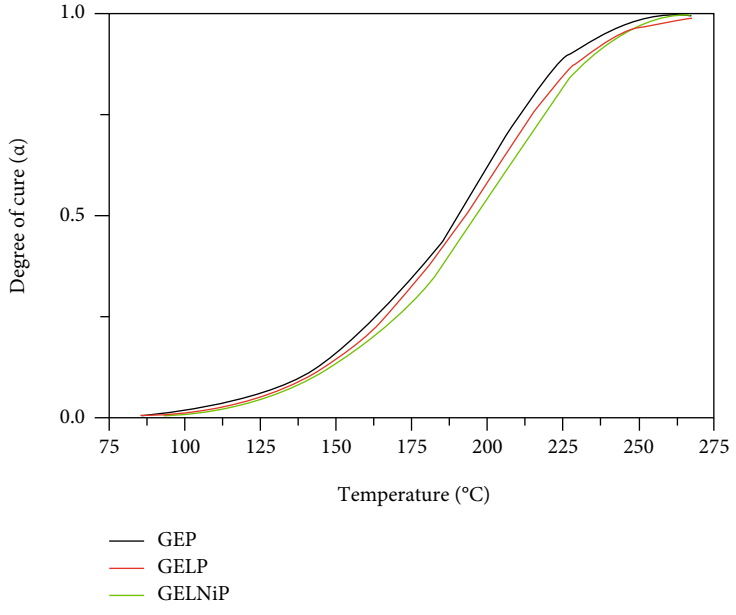

(d)

Figure 4: Conversion α as a function of temperatures for the system of GEP, GELP, and GELNiP at different heating rates of (a) 5, (b) 10, (c) 15, and (d) 20°C/min.

toward smaller values implying the accelerating role of LDH incorporation in the GEP curing reaction. This trend can be well described by the catalyst impact of LDH on opening the epoxy rings. Moreover, the variations in the shape of thermograms reveal the involvement of various curing mechanisms and kinetic parameters at the presence of LDH (Figure 4).

In comparison with LDH, the incorporation of LDH-$[Ni(EDTA)]^{2-}$ shifted T_p, $T_{o,}$ and T_e toward lower temperatures suggesting further acceleration of curing reaction upon the presence of the Ni(EDTA) complex intercalation of LDH. The amine groups and Ni ions in the interlayers of LDH-$[Ni(EDTA)]^{-2}$ further augmented the catalytic activities of LDH and promoted the primary amine–epoxide reaction.

3.3. Cure Analysis. Curing mechanisms and its kinetics modeling were addressed in this section for the epoxy prepregs containing 0.2 wt. % of LDH or LDH-$[Ni(EDTA)]^{-2}$.

3.3.1. Calculation of the Kinetic Parameters

(1) Friedman Model. The activation energies (E_α) can be determined by plotting $\ln(\varphi(d\alpha/dT))$ versus $1/T$, as shown

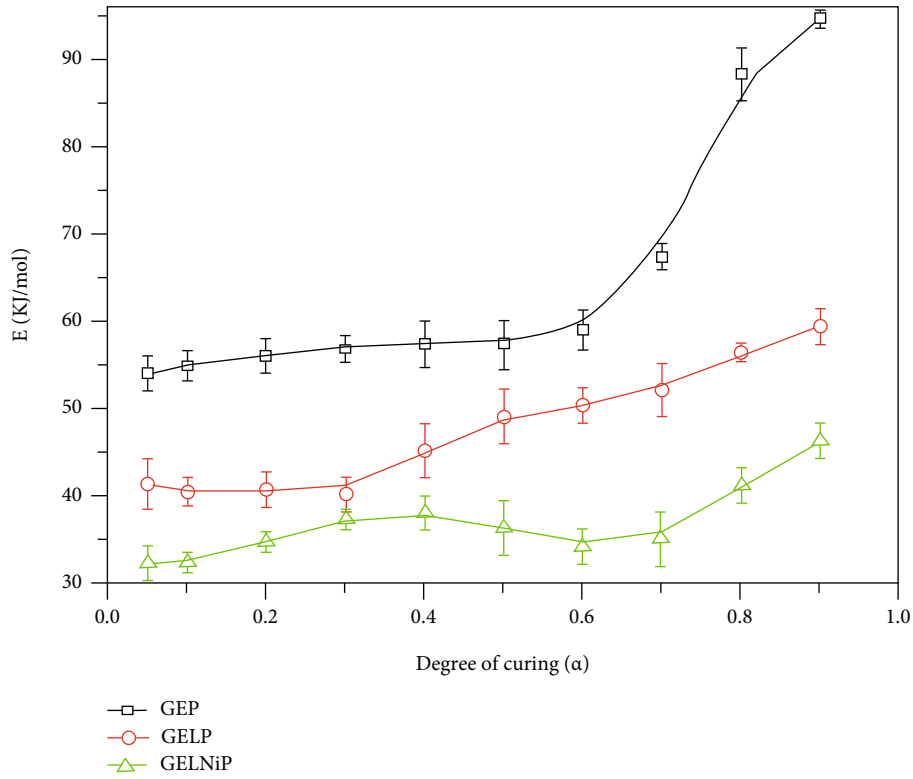

Figure 5: Variation of E_α versus conversion for GEP, GELP, and GELNiP nanocomposites derived from Friedman model.

in Figure 5. The slope of these plots is separately presented in Figure 6.

According to Figure 5, the curing trends of GEP, GELP, and GELNiP significantly differed. In the case of GEP, the apparent E_α remained constant at ~55 kJ/mol up to $\alpha = 0.6$ and then increases sharply toward the maximum value of 94 kJ/mol at a conversion of 90%. Concerning the GELP, at all degrees of curing, the apparent E_α was substantially lower than that of GEP. The E_α showed a decrement from ~60 kJ/mol at $\alpha = 0.05$ to a minimum of ~40 kJ/mol at $\alpha = 0.6$ followed by a rise to ~58 kJ/mol at $\alpha = 0.9$. In the case of the GELNiP system and for lower curing degrees ($\alpha < 0.2$), a rise in the curing degree slightly declined E_α to ~35 Kj/mol at $\alpha = 0.2$ which then remained almost constant until $\alpha = 0.9$. Here, E_α was evidently lower than those of GEP and GELP. The variations in E_α in the course of the curing process could be assigned to the following trend: temperature is lower at the early curing stages, and the reactions mainly occur between epoxy and amine groups. By the progression of the curing reaction, and hence at augmented temperatures, other reactions (mainly epoxy etherification, but hydroxyl are also probable) are expected to gain further importance [18, 35, 36]. The odd low activation energy of the nanocomposite at lower curing degrees confirmed the facilitating role of the LDH or LDH-$[Ni(EDTA)]^{-2}$ incorporation in the curing process, especially the initial epoxy-amine reaction. The first stages of the dependency of GEP are the characteristic of epoxy-amine reactions. At the final stages of the reaction, a decline in E_α values can be assigned to a transition from chemical control of the crosslinkers to the diffusive controls which had become evident in this system at the gelation stage. For GELP and GELNiP, the characteristic decrement of E_α was milder guiding use to this conclusion that its contribution is lower in this case. Side reactions (etherifications/homopolymerizations) are anticipated at higher temperatures; thus, it can be hypothesized that these reactions are significant in the case of GELNiP. Two reasons can justify the smaller activation energy of the LDH-$[Ni(EDTA)]^{-2}$ incorporated prepregs. First, the improvement in the dispersion of nanosheets in the epoxy matrix through galleries enlargement between LDH sheets due to the $[Ni(EDTA)]^{-2}$ intercalation of LDH layers. Ni ions in the interlayers of LDH nanosheets can also serve as catalysts and accelerate the reaction between the epoxy resin and curing agent. At the presence of $[Ni(EDTA)]^{-2}$ in the interlayers of LDH-$[Ni(EDTA)]^{-2}$ nanosheets, lower energies are required to achieve the epoxy-amine reaction which was proved by a decline in $E\alpha$ of GELNiP in comparison with GELP. It was proposed that the main curing reaction mechanism is addition of primary amine to the epoxide groups, accompanied with catalytic polymerization reaction of epoxide groups with the complex cation at the lower temperatures. The reactions of metal-containing and complex compounds with epoxy oligomers are examined in several works as mentioned the introduction part. Being ionic compounds, metal salts react with epoxy oligomers through the coordination of the cations with epoxy groups and the formation of a transition complex. The oxirane ring opening is accompanied by the formation of an ionic associate that acts as the initiator of ion polymerization.

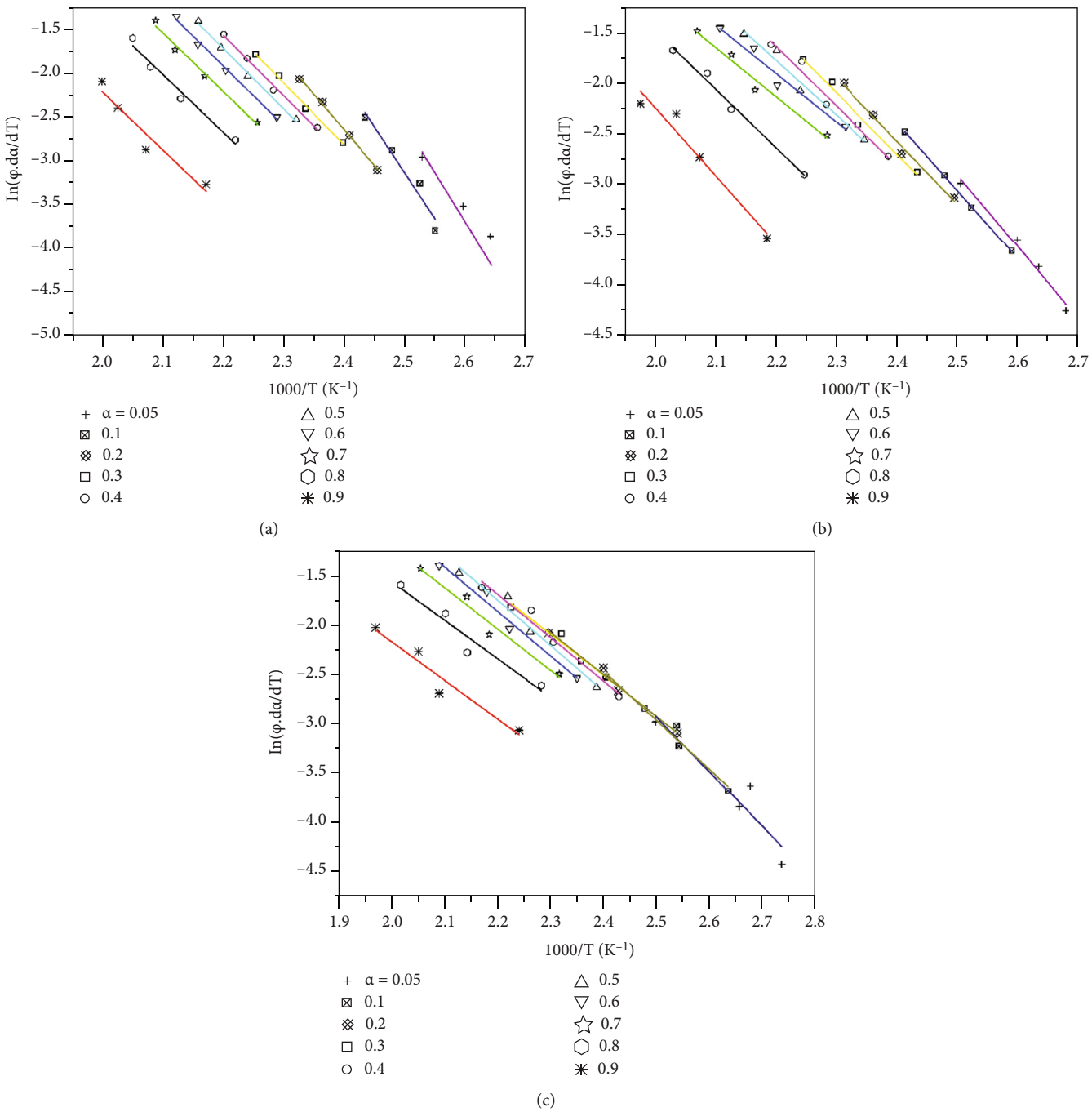

Figure 6: Typical plots of ln(dα/dt) vs. 1/T for (a) GEP, (b) GELP, and (c) GELNiP nanocomposites based on Friedman model at $\varphi = 5$°C/min.

The cure of epoxy resin with an amine curing agent occurs through several steps. The primary amines react with an epoxied ring, at the end of epoxy resin chains to form secondary amines at the beginning of curing reaction. With increasing in the viscose system, the reactivity and accessibility to oxirane groups become less and therefore, the crosslinking reaction of epoxy with the hydrogen of secondary amine starts to be more pronounce. Meanwhile, some hydroxyl groups form during the opening reaction between oxirane ring and the primary and secondary amine. These OH groups can also act as a catalyst in promoting the oxirane ring opening reaction at higher temperatures. Moreover, the kinetic of epoxy ring opening can be changed by Ni(II) known as lewis acid catalysis. It is supposed that the hardening of epoxy oligomers with the various chelates of nickel proceeds both at the expense of the reactions of the epoxy and hydroxyl groups with the alkoxy groups included into the compositions of the nickel chelates and due to the reaction of the ligands with the epoxy groups. The curing reaction proceeded through a two-step polymerization mechanism. The formation of 1 : 1 adduct between the epoxy resin and Nickel(II)-EDTA complex (first step) was followed by chain growth polymerization reaction (second step). The

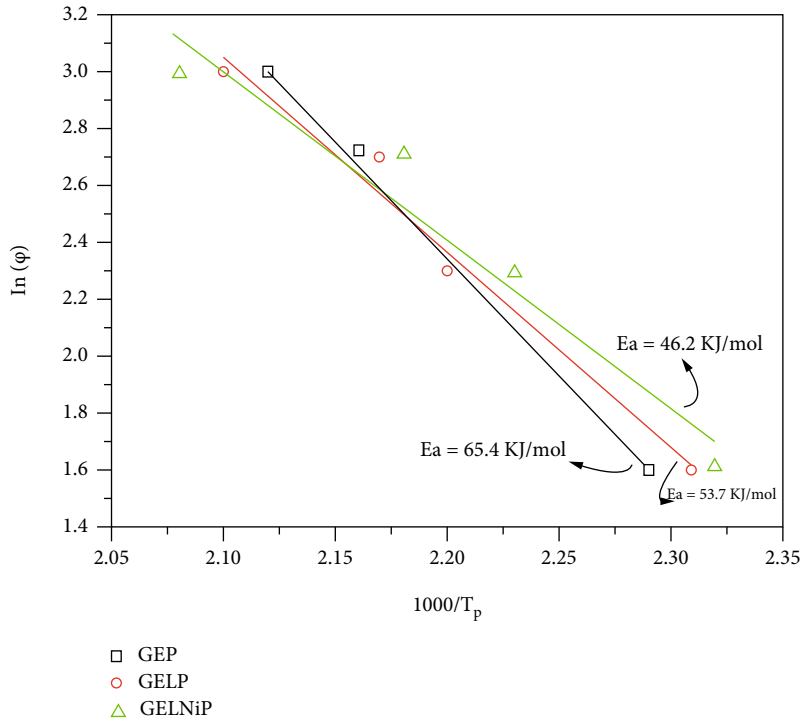

Figure 7: Plots of ln(Ø) vs. 1/T for GEP, GELP, and GELNiP nanocomposites derived from FWO model.

complex curing agent dissociates to form active cation species during the first stage of reaction. With increasing in temperature, the complex cation is dissociated completely. The dissociation equilibrium of the complex curing agent dissolved in epoxy resin at high temperatures. It is clear that complex curing agent is not capable of having an interaction with the epoxy groups due to deactivation of the amine groups, steric hindrance, and coordination number restriction. This means that other active species must be created in the reaction media to start the curing reaction. With raising the temperature, the active cationic species are produced owing to dissociation of the complex, that is more Ni–N, donor–acceptor, linkages are broken and more active amine sites will be available. It is interesting to note that active species are able to commence effective interactions with the epoxy groups by the amine addition reactions, and/or catalytic polymerization reaction (due to reduction of the coordination number of nickel to 4). It seems that there is a competition between catalytic polymerization reaction and amine addition reactions at the initial step of the curing reaction. However, the complex cation (II) is dissociated completely at elevated temperatures, and the polymerization is preceded by the amine addition reactions.

(2) FWO Method. Using the FWO method, the activation energy can be calculated from the slope of $\ln(\varphi)$ versus $1/T$, as depicted in Figure 7.

In this technique, the activation energy is independent of conversion. According to FWO, the values of activation energy were 65.4, 53.7, and 46.2 for the GEP, GELP, and GELNiP, respectively.

(3) KAS Method. A straight line will be achieved by plotting $\ln(\varnothing/T^{1.92})$ versus 1/T (see Figure 8) whose slope is the activation energy (Figure 9).

Similar to the Friedman model, the activation energy showed a reduction for the GEP system at the initial stages of curing. For epoxy/LDH and epoxy/LDH-$[Ni(EDTA)]^{2-}$, however, the activation energy remained constant over conversion when the KAS model was employed (Figure 9). The E_α of GELP and GELNiP was less than GEP which might be assigned to the improved reactivity of the system upon LDH and LDH-$[Ni\ (EDTA)]^{-2}$ incorporation.

Although the FR-obtained average activation energies (61.24, 48.8, and 35.8 kJ.mol^{-1} for GEP, GELP, and GELNiP, respectively) were more than those determined by the KAS (56.9, 40.5, and 27.3 kJ mol^{-1} for GEP, GELP, and GELNiP, respectively), both approaches predicted the same trend of the apparent activation energy. Therefore, both approaches can be implemented.

3.3.2. Determination of the Reaction Model. Determination of the reaction model parameters considering the role of pristine and $[Ni(EDTA)]^{-2}$ intercalated LDH in the curing mechanism is a prominent step in studies on the cure kinetics. Friedman and Malek methods were implemented to explore the reaction kinetics.

(1) Friedman Method. According to the Friedman method, the curing process of epoxy can be modeled by Eq. (5), assuming the n -th order reaction:

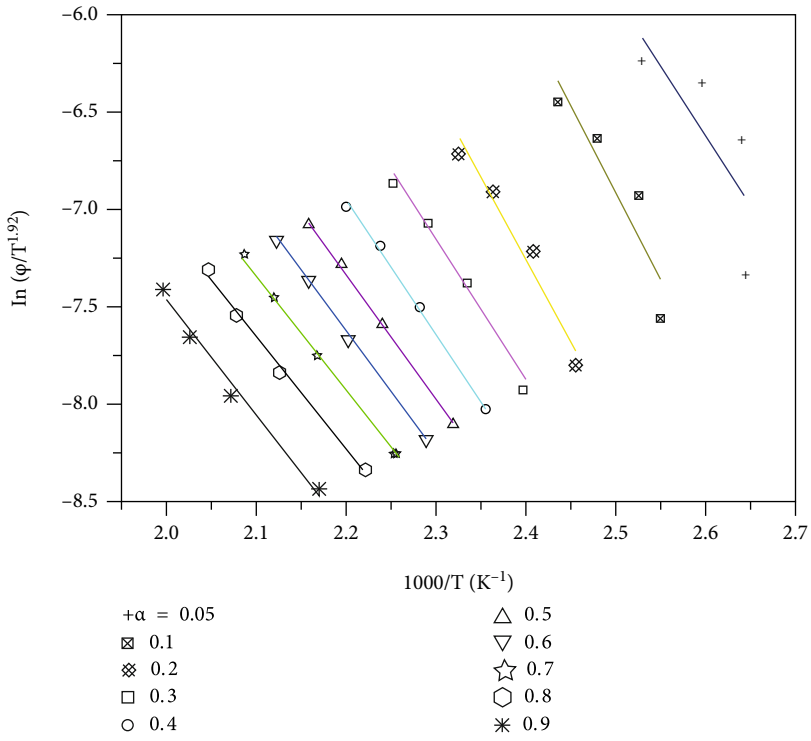

(a)

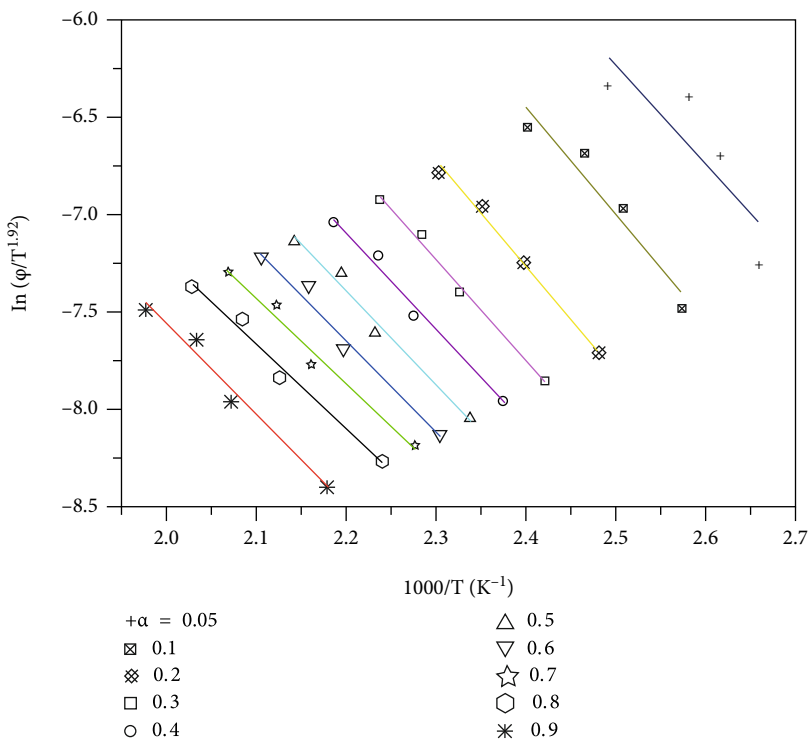

(b)

Figure 8: Continued.

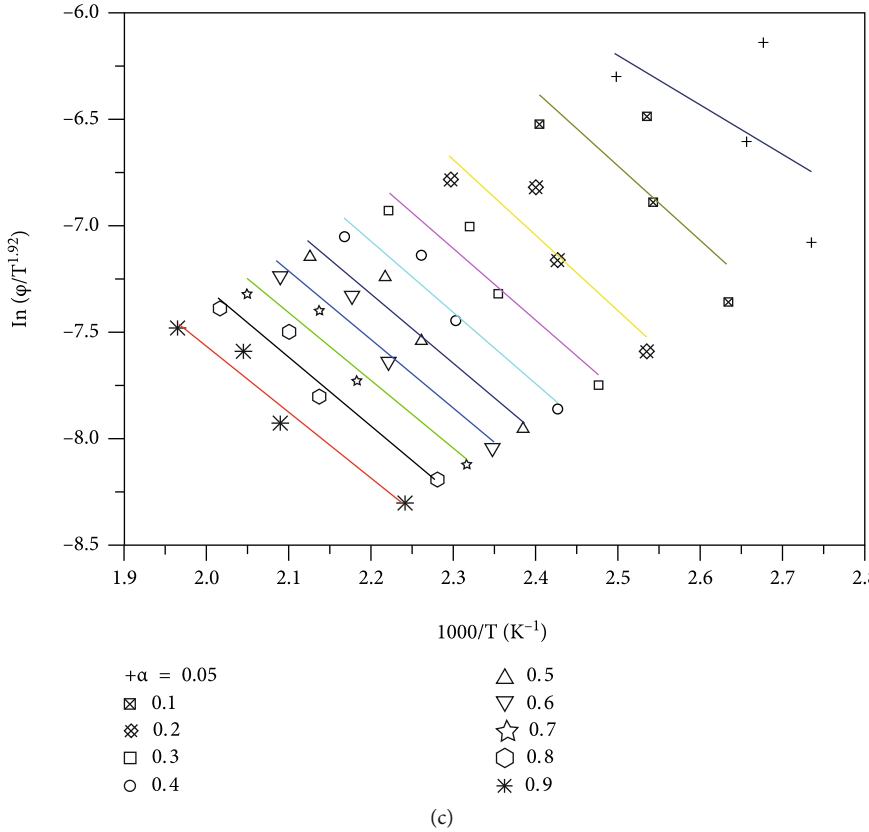

Figure 8: Plots of $\ln(\emptyset/T^{1.92})$ vs. 1/T for (a) GEP, (b) GELP, and (c) GELNiP nanocomposites based on KAS model.

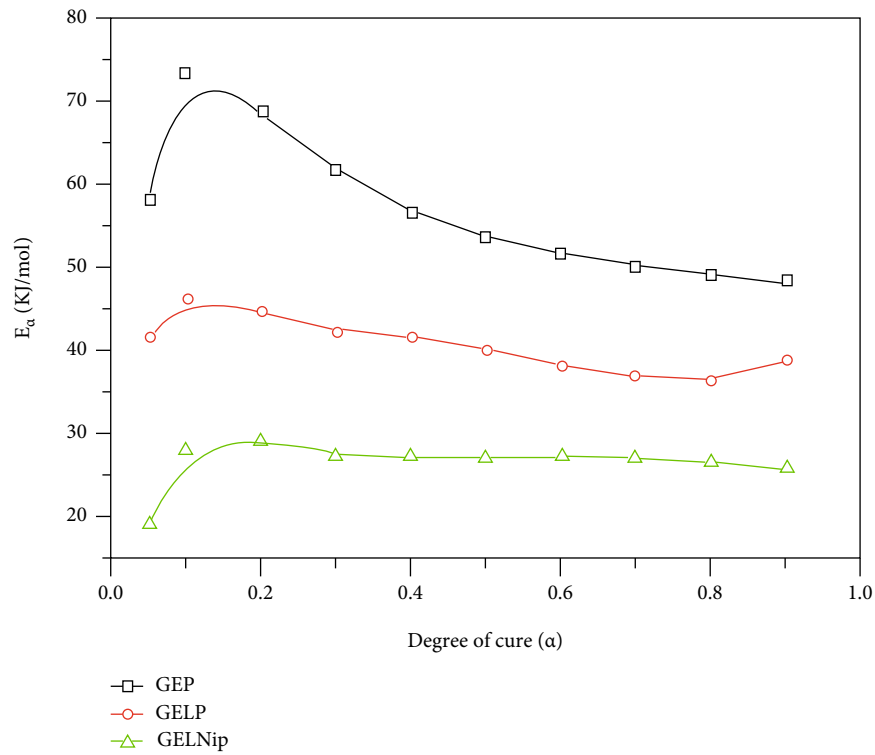

Figure 9: Variation of E_α versus conversion for GEP, GELP, and GELNiP nanocomposites derived from the KAS model.

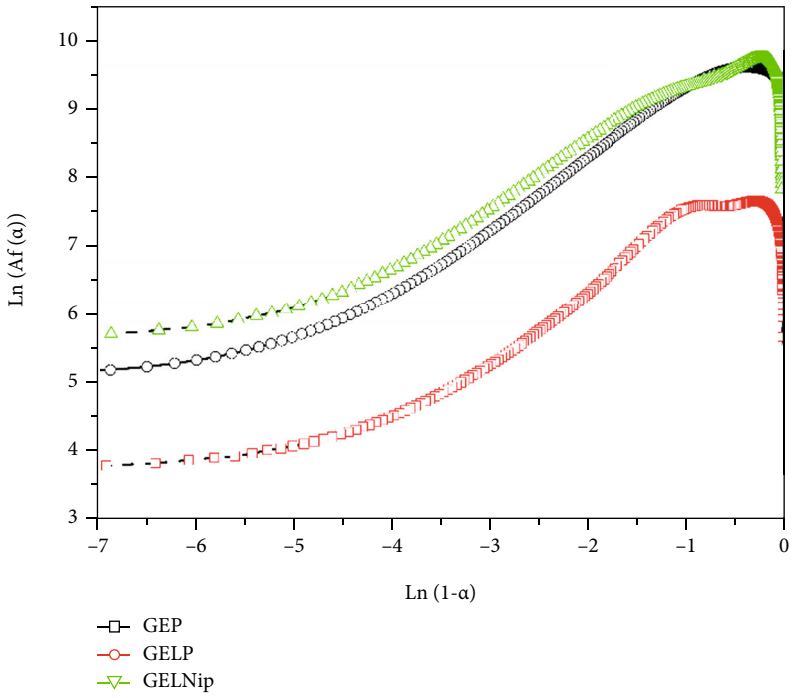

(a)

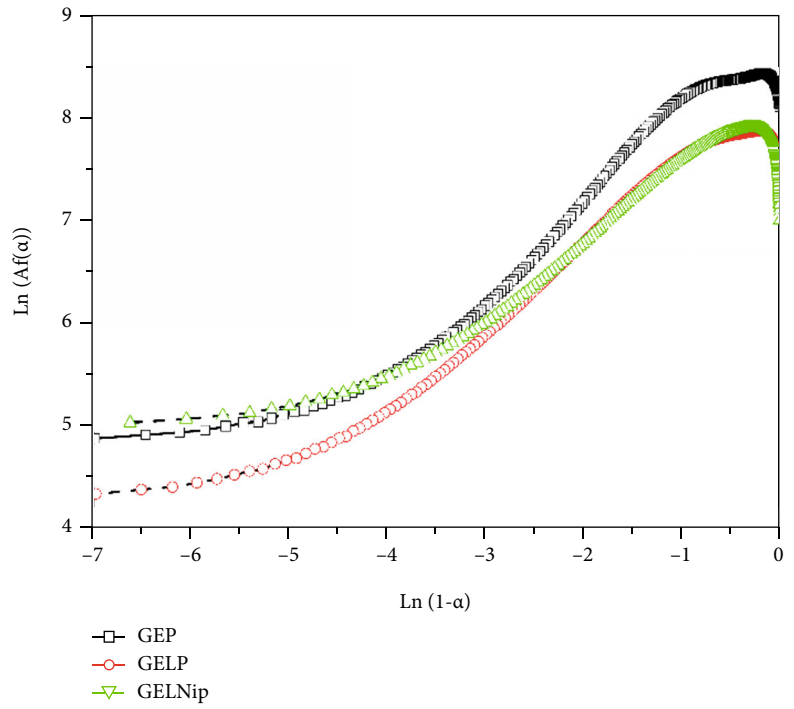

(b)

Figure 10: Continued.

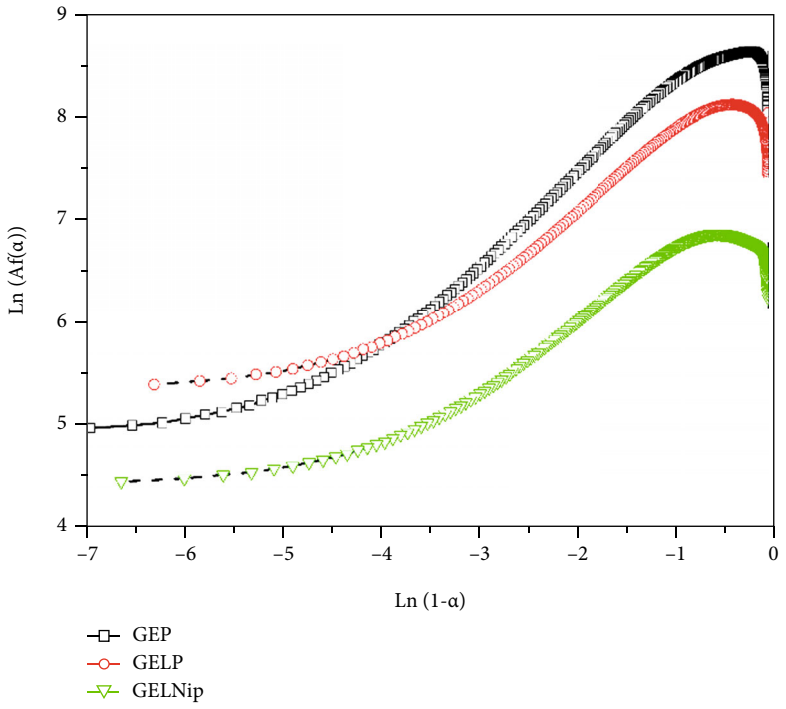

(c)

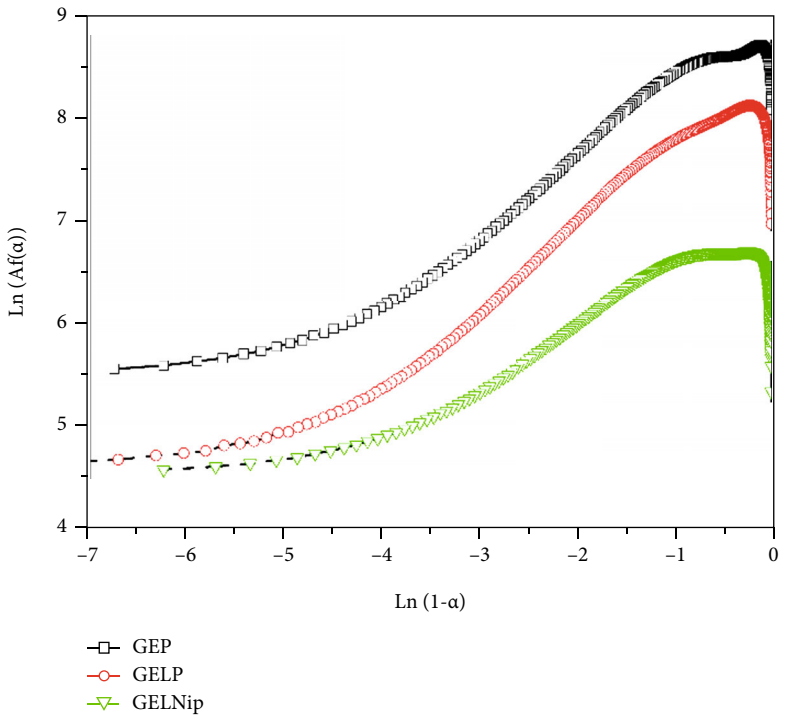

(d)

FIGURE 10: Typical plots of ln [Af(α)] vs. ln (1-α) for the samples under heating rate of 5°C.min^{-1} used in calculation of activation energy via Friedman method.

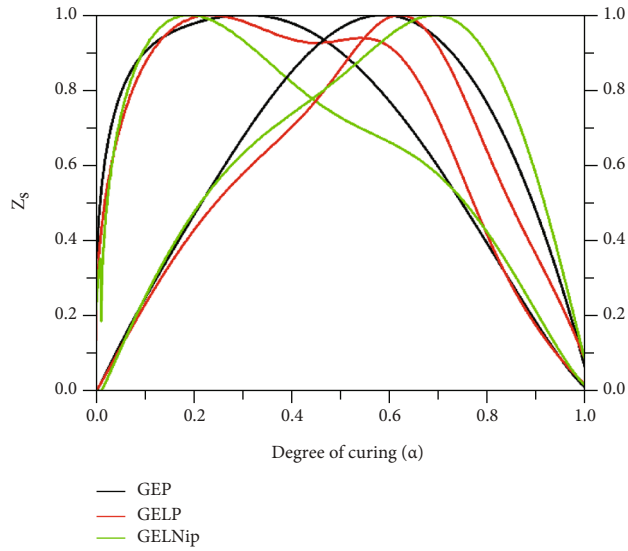

(a)

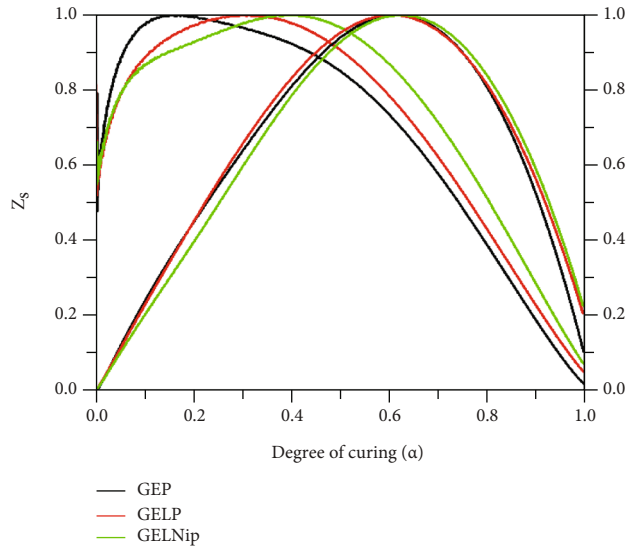

(b)

Figure 11: Continued.

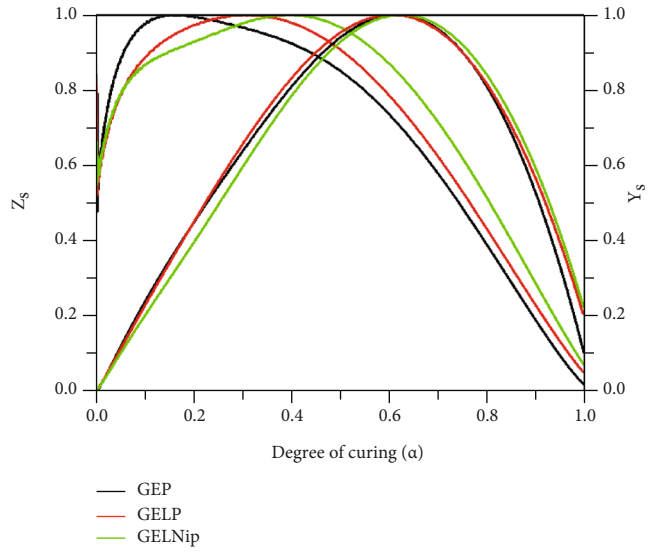

(c)

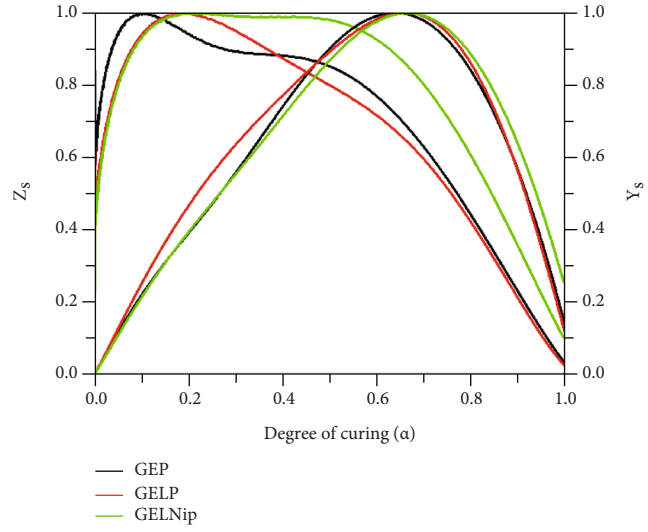

(d)

FIGURE 11: Typical plots of variation of $Y(\alpha)$ and $Z(\alpha)$ versus conversion for GEP, GELP, and GELNiP Ni nanocomposites based on the Malek model at heating rate of (a) 5, (b)10, (c) 15, and (d) 20°C/min.

$$\ln\left(Af(\alpha) = \ln\left(\frac{d\alpha}{dT}\varphi\right) + \frac{E_a}{RT} = \ln(A) + nln(1-\alpha).\right. \quad (5)$$

The shape of ln [Af(α)] versus ln (1-α) indicates the deviation from the n-th order reaction (Figure 10).

For the n -th-order cure reaction, a straight line was observed when ln [Af(α)] was plotted against ln (1-α) whose slope is the reaction order (n). Based on Figure 10, a maximum can be observed in the conversion between values of 0.1 and 0.5 which is typical for autocatalytic reactions.

(2) Malek Method. The following equations can be employed to determine the kinetic model based on the Malek method:

$$Y(\alpha) = \frac{d\alpha}{dt} \times \exp\left(\frac{E_a}{RT}\right) = Af(\alpha), \quad (6)$$

$$Z(\alpha) = \frac{d\alpha}{dt} \times T^2\left(\frac{\pi}{\beta T}\right), \quad (7)$$

where π indicates the function of temperature integrals which can be sufficiently approximated with the following expression [(7)]:

Table 1: The kinetic parameters of the curing of GEP, GELP, and GELNiP based on the FR and KAS model at various heating rates.

Samples		5 K/min		10 K/min		15 K/min		20 K/min		Mean	
		FR	KAS	FR	KAS	FR	KAS	FR	KAS	FR	KAS
GEP	E_α									61.2	56.9
	LnA	10.34	8.4	9.43	10.02	9.3	9.67	9.4	8.9	9.6	9.24
	m	0.24	0.32	0.29	0.27	0.25	0.29	0.23	0.31	0.25	0.29
	n	1	1.06	1.22	1.14	1.04	1.25	0.95	1.01	1.05	1.11
GELP	E_α									48.8	40.5
	LnA	9.2	8.1	8.6	7.8	8.71	7.84	8.78	7.9	8.8	7.91
	m	0.45	0.34	0.32	0.38	0.31	0.27	0.31	0.29	0.35	0.32
	n	1.43	1.2	1.03	0.98	0.97	0.82	0.99	1.03	1.1	1
GELNiP	E_α									35.8	27.3
	LnA	10.53	0.76	8.55	0.67	7.4	0.7	7.3	0.68	8.44	0.7
	m	0.36	0.28	0.37	0.34	0.33	0.31	0.3	0.29	0.34	0.3
	n	0.97	1.03	1	1.2	0.9	0.83	0.8	0.91	0.92	0.99

Table 2: The values of α_p, α_m, and $\alpha_p^{\inf}$ obtained from DSC analysis based on the Malek model at various heating rates.

Samples		5 K/min	10 K/min	15 K/min	20 K/min	$\gamma = \alpha_{mav}/(1-\alpha_{mav})$
GEP	$\alpha_p^{\inf}$	0.598	0.624	0.618	0.644	0.24
	α_p	0.564	0.596	0.58	0.619	
	α_m	0.31	0.168	0.18	0.116	
GELP	$\alpha_p^{\inf}$	0.625	0.634	0.612	0.674	0.31
	α_p	0.624	0.608	0.541	0.632	
	α_m	0.241	0.201	0.319	0.197	
GELNiP	$\alpha_p^{\inf}$	0.704	0.619	0.627	0.668	0.37
	α_p	0.679	0.574	0.59	0.637	
	α_m	0.201	0.246	0.407	0.217	

$$\pi = \frac{(E_\alpha/RT)^3 + 18(E_\alpha/RT)^2 + 88(E_\alpha/RT) + 96}{(E_\alpha/RT)^4 + 20(E_\alpha/RT)^3 + 120(E_\alpha/RT)^2 + 240(E_\alpha/RT) + 120}. \quad (8)$$

In Eq. (8), E0 can be obtained using the FWO method in which the variations in the activation energy remain constant in terms of α. Both $Y(\alpha)$ and $Z(\alpha)$ functions were normalized within (0, 1) intervals:

$$Y_s(\alpha) = \frac{Y(\alpha)}{\text{Max}\,(Y_0(\alpha))}, \qquad Z_s(\alpha) = \frac{Z(\alpha)}{\text{Max}\,(Z_0(\alpha))}. \quad (9)$$

Considering the shape and the maximum values of $Y_s(\alpha)$ and $Z_s(\alpha)$, the best kinetic model can be selected. Then, the kinetic parameters such as n and m can be determined. Figure 11 depicts the changes in $Y_s(\alpha)$ and $Z_s(\alpha)$ with conversion α. $Y_s(\alpha)$ and $Z_s(\alpha)$ showed maximum values at α_m and $\alpha_p^{\inf}$, respectively. Furthermore, α_p can be determined using the DSC peak, as listed in Table 1.

Based on Figure 11 and Table 1, the curing process could be well described by a two-parameter autocatalytic kinetic model of Sesták–Berggren [37]. The average α_m, α_{mav}, was employed to determine the kinetic parameters. The general kinetic model can be rearranged in terms of the ratio of reaction order, $\gamma = (m/n)$ as mentioned by Málek:

$$\ln\left(\frac{d\alpha}{dT}\varphi e^{\frac{E_a}{RT}}\right) = Ln A + n\ln(\alpha^\gamma(1-\alpha)), \qquad \gamma = \frac{m}{n} = \frac{\alpha_{mav}}{1-\alpha_{mav}}, \quad (10)$$

where α_{Mav} shows the average α_M values. The values of α_p, α_m, and $\alpha_p^{\inf}$ obtained from DSC analysis based on the Malek model at various heating rates were shown in Table 2. The value of n as degree of noncatalytic and m as the degree of autocatalytic reactions as well as the

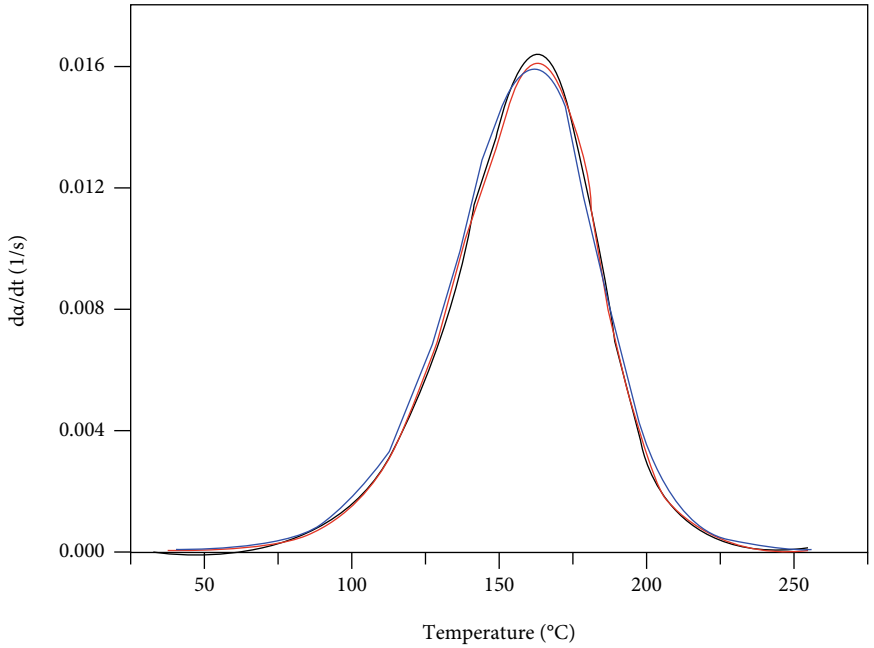

(a)

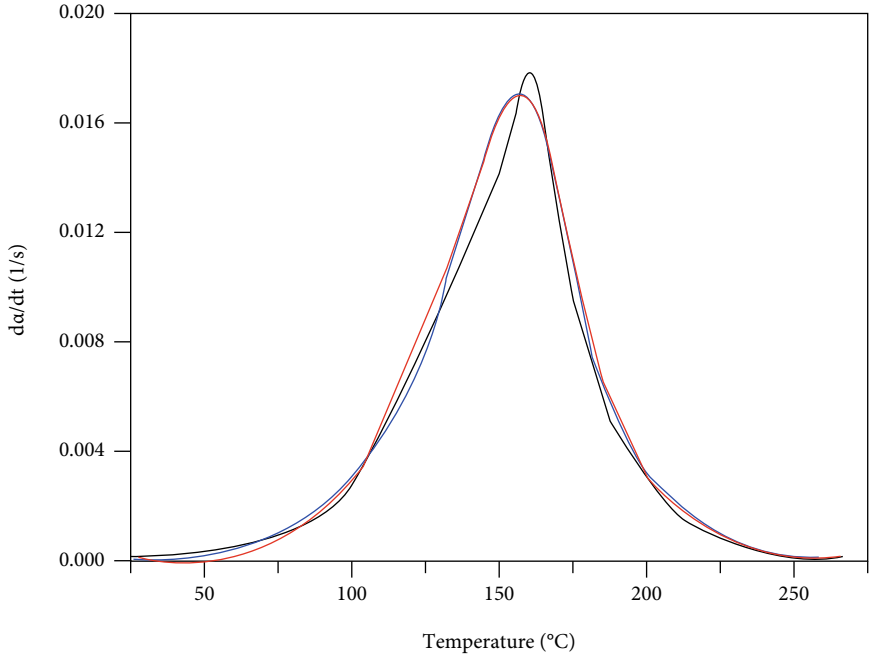

(b)

Figure 12: Continued.

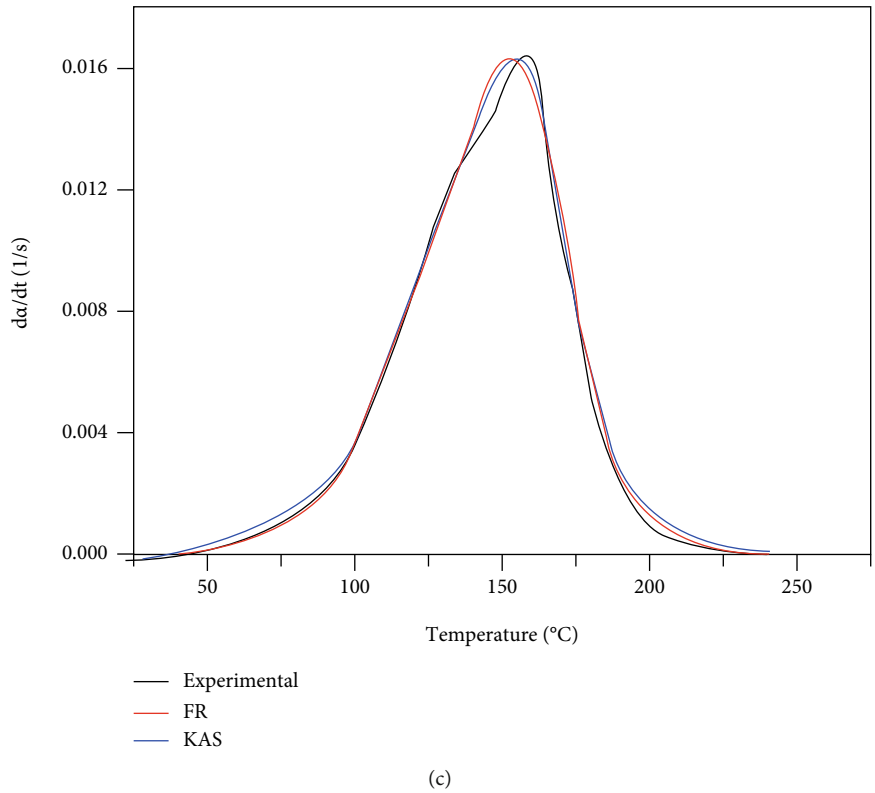

(c)

Figure 12: Comparison of experimental data with the kinetic models for (a) GEP, (b) GELP, and (c) GELNiP at heating rate of 5°C/min based on the Friedman and KAS model.

preexponential factor (A) was calculated by plotting ln $((d\alpha/\mathrm{dT})\varphi e^{E_a/RT})$ against ln $(\alpha^{\gamma}(1-\alpha))$.

The kinetic parameters (E_α, n, and m) and the mean E_α of various conversions were applied in the Friedman and Malek methods as tabulated in Table 1.

Based on Table 1, the kinetic parameters (n, m, and LnA) offered by the Friedman method are properly in line with those of the KAS method. The kinetic parameters showed an increase in the autocatalytic reaction order (m) upon the incorporation of LDH and LDH-$[Ni(EDTA)]^{2-}$ indicating a shift in the mechanism from noncatalytic to autocatalytic. Furthermore, the use of LDH and LDH-$[Ni(EDTA)]^{2-}$ nanosheets enhanced the collisions between the reaction moieties, thus raising the pre-exponential factor.

3.3.3. Model Validation. The Málek method was validated by comparing the plots of $d\alpha/dT$ vs. T for the data of Table 1 and experimental data. The results of the comparison are presented in Figure 12 for GEP, GELP, and GELNiP. Finally, the kinetic parameters were validated by comparing the plots of $d\alpha/dT$ against T for the data of Table 1 and experimental values. Figure 12 presents the reliability of the analytical curing rate for neat epoxy, epoxy/LDH, and epoxy/LDH-$[Ni\ (EDTA)]^{2-}$ according to the Friedman and KAS methods, respectively.

As can be seen, both Friedman and KAS approaches well agreed with the experimental findings with some minor differences at the advanced stages of the curing reaction. At the initial crosslinking stages, the viscosity of the system was low, and the curing process was under the control of the chemical kinetics prior to the gelation. Before gelation and vitrification, the curing rate could be well described by Friedman and KAS techniques. Besides that, some deviation emerged between the empirical and predicted values when the curing reaction continued which can be assigned to the rise of viscosity. After gelation and vitrification, the mobility of curing reactant decreases and the crosslinking reaction becomes diffusion-controlled decreased and the crosslinking reaction was controlled.

4. Conclusion

The cure kinetics of GEP was evaluated with and without LDH or LDH-$[Ni(EDTA)]^{-2}$ using nonisothermal DSC. The presence of LDH altered the cure temperature toward lower values and accelerated the GEP curing. The incorporation of LDH-$[Ni(EDTA)]^{-2}$ played a more pronounced role in accelerating the GEP curing. Activation energies were determined by the differential isoconversional approach of FR and the integral techniques of FWO and KAS. The activation energy showed a declining trend upon the incorporation of LDH or LDH-$[Ni(EDTA)]^{-2}$ at low curing degrees indicating the stronger influence of LDH on the curing process. LDH facilitated the curing reaction, especially in the initial epoxy/amine reaction. Furthermore, $[Ni(EDTA)]^{-2}$ complex intercalated LDH manifested superior performance. The activation energy of the neat epoxy prepreg (GEP) exhibited a descending pattern against the conversion of the system. The average activation energy decreased from 58 kJ/mol for GEP to 42 kJ/mol for LDH-

containing GELP which was further reduced to 32 kJ/mol upon the use of LDH-[Ni (EDTA)]$^{-2}$. Such a further decrease in the LDH-[Ni (EDTA)]$^{2-}$-incorporated epoxy prepreg compared to the LDH-containing system can be explained by the contribution of Ni ions in the interlayer of LDH nanosheets to opening the epoxy rings which catalyzed the curing reaction. The autocatalytic model was employed to explain the cure kinetics of the investigated systems. Upon the incorporation of the LDH or LDH-[Ni (EDTA)]$^{-2}$, the Sesták–Berggren model still managed to describe the cure kinetic of GEP composites, as its results were in line with the empirical data. Additionally, the Sesták–Berggren model was applied to propose the kinetic parameters and the equation of the curing process.

Data Availability

The data used to support the findings of this study are available from the corresponding author upon request.

Conflicts of Interest

The authors declare that they have no conflicts of interest.

References

[1] S. R. Karnati, P. Agbo, and L. Zhang, "Applications of silica nanoparticles in glass/carbon fiber-reinforced epoxy nanocomposite," *Composites Communications*, vol. 17, pp. 32–41, 2020.

[2] J. Morancho, X. Ramis, X. Fernández-Francos, J. Salla, A. O. Konuray, and À. Serra, "Curing of off-stoichiometric amine–epoxy thermosets," *Journal of Thermal Analysis and Calorimetry*, vol. 133, no. 1, pp. 519–527, 2018.

[3] L. Granado, S. Kempa, L. J. Gregoriades et al., "Kinetic regimes in the curing process of epoxy-phenol composites," *Thermochimica acta.*, vol. 667, pp. 185–192, 2018.

[4] A. Ganapathi, S. C. Joshi, and Z. Chen, "Influence of cure kinetic, rheological and thermo-mechanical behavior on micro-level curing strain of an epoxy prepreg," *Journal of Thermal Analysis and Calorimetry*, vol. 124, no. 1, pp. 305–316, 2016.

[5] P. K. Mohan, A. K. M, S. G. kumar, and P. M. Mohite, "Development of in-house unidirectional carbon/epoxy prepregs and its characterization for aerospace applications," *Procedia Structural Integrity*, vol. 14, pp. 176–183, 2019.

[6] P. Vijayan P, D. Puglia, H. Rastin, M. R. Saeb, B. Shojaei, and K. Formela, "Cure kinetics of epoxy/MWCNTs nanocomposites: isothermal calorimetric and rheological analyses," *Progress in Organic Coatings*, vol. 108, pp. 75–83, 2017.

[7] M. Jouyandeh, M. R. Ganjali, J. A. Ali et al., "Curing epoxy with polyethylene glycol (PEG) surface-functionalized Gd Fe3-O4 magnetic nanoparticles," *Progress in Organic Coatings*, vol. 137, article 105283, 2019.

[8] F. Tikhani, S. Moghari, M. Jouyandeh et al., "Curing kinetics and thermal stability of epoxy composites containing newly obtained nano-scale aluminum hypophosphite (AlPO2)," *Polymers*, vol. 12, no. 3, p. 644, 2020.

[9] L. Gao, Q. Zhang, J. Guo et al., "Effects of the amine/epoxy stoichiometry on the curing behavior and glass transition temperature of MWCNTs-NH_2/epoxy nanocomposites," *Thermochimica Acta.*, vol. 639, pp. 98–107, 2016.

[10] T. Li, H. N. Miras, and Y.-F. Song, "Polyoxometalate (POM)-layered double hydroxides (LDH) composite materials: design and catalytic applications," *Catalysts*, vol. 7, no. 9, p. 260, 2017.

[11] H. Rastin, M. R. Saeb, M. Nonahal et al., "Transparent nanocomposite coatings based on epoxy and layered double hydroxide: nonisothermal cure kinetics and viscoelastic behavior assessments," *Progress in Organic Coatings.*, vol. 113, pp. 126–135, 2017.

[12] M. J. Mochane, S. I. Magagula, J. S. Sefadi, E. R. Sadiku, and T. C. Mokhena, "Morphology, thermal stability, and flammability properties of polymer-layered double hydroxide (LDH) nanocomposites: a review," *Crystals*, vol. 10, no. 7, p. 612, 2020.

[13] C. Prasad, H. Tang, and W. Liu, "Magnetic Fe3O4 based layered double hydroxides (LDHs) nanocomposites (Fe3O4/LDHs): recent review of progress in synthesis, properties and applications," *Journal of Nanostructure in Chemistry.*, vol. 8, no. 4, pp. 393–412, 2018.

[14] X. He, T. Li, Z. Shi et al., "Thermal-oxidative aging behavior of nitrile-butadiene rubber/functional LDHs composites," *Polymer Degradation and Stability.*, vol. 133, pp. 219–226, 2016.

[15] S. Naseem, S. P. Lonkar, A. Leuteritz, and F. J. W. Labuschagné, "Different transition metal combinations of LDH systems and their organic modifications as UV protecting materials for polypropylene (PP)," *RSC Advances*, vol. 8, no. 52, pp. 29789–29796, 2018.

[16] M. R. Sovizi, G. Fakhrpour, and A. R. Madram, "Comparison of thermal degradation behavior of epoxy/ammonium perchlorate composite propellants," *Journal of Thermal Analysis and Calorimetry.*, vol. 129, no. 1, pp. 401–410, 2017.

[17] M. Chen, S. Peng, M. Zhao, Y. Liu, and C. Liu, "The curing and degradation kinetics of modified epoxy–SiO 2 composite," *Journal of Thermal Analysis and Calorimetry.*, vol. 130, no. 3, pp. 2123–2131, 2017.

[18] M. Jouyandeh, S. M. R. Paran, S. S. M. Khadem et al., "Nonisothermal cure kinetics of epoxy/$Mn_xFe_{3-x}O_4$ nanocomposites," *Progress in Organic Coatings*, vol. 140, article 105505, 2020.

[19] M. Jouyandeh, Z. Karami, S. M. Hamad et al., "Nonisothermal cure kinetics of epoxy/Zn Fe3-O4 nanocomposites," *Progress in Organic Coatings*, vol. 136, article 105290, 2019.

[20] M. Ganjaee Sari, H. Vahabi, X. Gabrion et al., "An attempt to mechanistically explain the viscoelastic behavior of transparent epoxy/starch-modified ZnO nanocomposite coatings," *Progress in Organic Coatings*, vol. 119, pp. 171–182, 2018.

[21] V. Yuste-Sánchez, M. Hernández Santana, T. A. Ezquerra, R. Verdejo, and M. A. López-Manchado, "In-situ cure monitoring of epoxy/graphene nanocomposites by several spectroscopic techniques," *Polymer Testing*, vol. 80, article 106114, 2019.

[22] M. R. Saeb, H. Rastin, M. Nonahal, S. M. R. Paran, H. A. Khonakdar, and D. Puglia, "Cure kinetics of epoxy/chicken eggshell biowaste composites: isothermal calorimetric and chemorheological analyses," *Progress in Organic Coatings.*, vol. 114, pp. 208–215, 2018.

[23] M. Nonahal, H. Rastin, M. R. Saeb et al., "Epoxy/PAMAM dendrimer-modified graphene oxide nanocomposite coatings: nonisothermal cure kinetics study," *Progress in Organic Coatings.*, vol. 114, pp. 233–243, 2018.

[24] G. Gerami, R. Bagheri, and R. Darvishi, "Investigation of isothermal and dynamic cure kinetics of epoxy resin/nadic

methyl anhydride/dicyandiamide by differential scanning calorimetry (DSC)," *Journal of Thermal Analysis and Calorimetry.*, vol. 137, no. 2, pp. 575–582, 2019.

[25] M. R. Saeb, M. Nonahal, H. Rastin et al., "Calorimetric analysis and molecular dynamics simulation of cure kinetics of epoxy/chitosan-modified Fe_3O_4 nanocomposites," *Progress in Organic Coatings.*, vol. 112, pp. 176–186, 2017.

[26] J. D. Thanki and P. H. Parsania, "Dynamic DSC curing kinetics and thermogravimetric study of epoxy resin of 9, 9′-bis (4-hydroxyphenyl) anthrone-10," *Journal of Thermal Analysis and Calorimetry.*, vol. 130, no. 3, pp. 2145–2156, 2017.

[27] K. Leena, P. Soumyamol, M. Baby, S. Suraj, R. Rajeev, and D. S. Mohan, "Non-isothermal cure and decomposition kinetics of epoxy–imidazole systems," *Journal of Thermal Analysis and Calorimetry*, vol. 130, no. 2, pp. 1053–1061, 2017.

[28] M. Jouyandeh, S. M. R. Paran, A. Jannesari, D. Puglia, and M. R. Saeb, "Protocol for nonisothermal cure analysis of thermoset composites," *Progress in Organic Coatings*, vol. 131, pp. 333–339, 2019.

[29] Z. Karami, M. Jouyandeh, J. A. Ali et al., "Epoxy/layered double hydroxide (LDH) nanocomposites: synthesis, characterization, and _Excellent_ cure feature of nitrate anion intercalated Zn-Al LDH," *Progress in Organic Coatings*, vol. 136, article 105218, 2019.

[30] M. Hayaty, M. H. Beheshty, and M. Esfandeh, "Cure kinetics of a glass/epoxy prepreg by dynamic differential scanning calorimetry," *Journal of Applied Polymer Science.*, vol. 120, no. 1, pp. 62–69, 2011.

[31] M. Hayaty, H. Honarkar, and M. H. Beheshty, "Curing behavior of dicyandiamide/epoxy resin system using different accelerators," *Iranian Polymer Journal.*, vol. 22, no. 8, pp. 591–598, 2013.

[32] M. Pérez, I. Pavlovic, C. Barriga, J. Cornejo, M. Hermosín, and M. Ulibarri, "Uptake of Cu^{2+}, Cd^{2+} and Pb^{2+} on Zn-Al layered double hydroxide intercalated with edta," *Applied Clay Science*, vol. 32, no. 3-4, pp. 245–251, 2006.

[33] J. Li, L. Yan, Y. Yang, X. Zhang, R. Zhu, and H. Yu, "Insight into the adsorption mechanisms of aqueous hexavalent chromium by EDTA intercalated layered double hydroxides: XRD, FTIR, XPS, and zeta potential studies," *New Journal of Chemistry.*, vol. 43, no. 40, pp. 15915–15923, 2019.

[34] X. Tang, Y. Liu, and S. Li, "Heterogeneous UV-Fenton photodegradation of azocarmine B over [FeEDTA]− intercalated ZnAl-LDH at circumneutral pH," *RSC advances.*, vol. 6, no. 84, pp. 80501–80510, 2016.

[35] P. Nogueira, C. Ramirez, A. Torres et al., "Effect of water sorption on the structure and mechanical properties of an epoxy resin system," *Journal of Applied Polymer Science*, vol. 80, no. 1, pp. 71–80, 2001.

[36] M. Jouyandeh, E. Yarahmadi, K. Didehban et al., "Cure kinetics of epoxy/graphene oxide (GO) nanocomposites: effect of starch functionalization of GO nanosheets," *Progress in Organic Coatings*, vol. 136, article 105217, 2019.

[37] L. Lu, L. Xia, H. Zengheng, S. Xingyue, Z. Yi, and L. Pan, "Investigation on cure kinetics of epoxy resin containing carbon nanotubes modified with hyper-branched polyester," *RSC Advances*, vol. 8, no. 52, pp. 29830–29839, 2018.